



# Impacts of the South Asian high on tropical cyclone genesis in the South China Sea

Chao Wang<sup>1,2</sup> · Bin Wang<sup>2,3</sup>

Received: 2 June 2020 / Accepted: 14 December 2020 / Published online: 21 January 2021  
© The Author(s), under exclusive licence to Springer-Verlag GmbH, DE part of Springer Nature 2021

## Abstract

As a semi-permanent circulation system at the upper troposphere, the South Asian high (SAH) profoundly influences the Asian climate. However, its impact on the underlying tropical cyclone (TC) genesis in the South China Sea (SCS) remains unknown. Here we show that the leading mode of eastern-central SAH and TC genesis (TCG) number in the SCS during July–September are significantly correlated with a correlation coefficient of  $-0.71$  during 1979–2017. During the strong SAH years, the SAH-related upper-level convergence favors descending motion and low-level divergence in the SCS, decreasing mid-level humidity and low-level vorticity and thus suppressing TCG in the SCS. We find that the variations in the leading mode of eastern-central SAH are coupled to the meridional gradient in surface temperature over the western North Pacific. An enhanced meridional surface temperature gradient can increase the meridional gradient in 200 hPa geopotential height and thus intensify the SAH. Meanwhile, the intensified SAH and the related descending motion, in turn, re-enforce the meridional surface temperature gradient through positive SST-cloud-shortwave radiation feedback. The positive feedback between the SAH and the WNP meridional temperature gradients provides persisting large-scale circulation anomalies that influence the TCG in the SCS from July through September. These results highlight the importance of the SAH and its interaction with the WNP meridional temperature gradients for regulating the SCS TCG and suggest that the precursors that are known to be linked to the SAH intensity can be used to the seasonal prediction of TCG in the SCS.

## 1 Introduction

About one-third of tropical cyclones (TCs) that influence China are originated in the South China Sea (SCS) (Wang et al. 2007). TCs formed in the SCS usually bring massive disasters to peoples in adjacent countries (Zhang et al. 2009; Peduzzi et al. 2012; Kossin et al. 2016). Therefore, a comprehensive understanding of the variability of TC genesis (TCG) in the SCS would greatly help improvement of

TC prediction and disaster mitigation in the surrounding countries.

TCG in the SCS is tightly linked to the Asian monsoon circulation. TCs mainly originate in the northern (southern) SCS during the summer (winter) monsoon regime (Wang et al. 2007; Zuki and Lupo 2008). On the interannual time scale, El Niño–Southern Oscillation (ENSO) was found to have a profound impact on TCG in the SCS (Wang and Chan 2002; Zuki and Lupo 2008; Goh and Chan 2010; Chen 2011; Du et al. 2011; Wang et al. 2014). Generally, there is an enhanced TCG in the late season during La Nina developing phase but a suppressed TCG in the late season during El Niño developing phase in the SCS (Wang and Chan 2002; Wang et al. 2007). However, Goh and Chan (2010) pointed out that TCG frequency in the SCS shows no significant difference between two phases of ENSO in the summer season. While these studies mainly focused on the SCS TC activity in developing phases of ENSO, Du et al. (2011) found that TCG frequency in the SCS tends to increase in summers following strong El Niño events due to the reduced vertical wind shear. Besides influences of ENSO, sea surface temperature (SST) in the North Indian Ocean also can modulate the

✉ Chao Wang  
wangchao.typhoon@gmail.com; wangchao@nuist.edu.cn

<sup>1</sup> Key Laboratory of Meteorological Disaster of Ministry of Education, Joint International Research Laboratory of Climate and Environment Change and Collaborative Innovation Center On Forecast and Evaluation of Meteorological Disasters, Nanjing University of Information Science and Technology, Nanjing, China

<sup>2</sup> Earth System Modeling Center, Nanjing University of Information Science and Technology, Nanjing, China

<sup>3</sup> Department of Atmospheric Sciences and International Pacific Research Center, University of Hawaii at Manoa, Honolulu, HI 96822, USA

SCS TCG by changing large-scale conditions (Wang et al. 2013; Li and Zhou 2014). However, variability sources of the SCS TCG are far from being fully understood because of the weak relationship between the local large-scale conditions and TCG in the SCS in summer. Particularly, changes in dynamical environmental parameters usually play an important role in the interannual variability of SCS TCG, while variations in thermodynamic ones have little contribution since the thermodynamic thresholds for TCG are always satisfied over the SCS in summer (Wang et al. 2007).

As an alternative to understanding TCG in terms of large-scale parameters, some large-scale circulations can provide a more comprehensive perspective to interpret variabilities in TCG (Briegel and Frank 1997; Wu et al. 2015; Wang and Wu 2016, 2018a, b; Wang and Wang 2019). Most of TCG in the SCS occurs to the southern flank of the upper-level South Asian high (SAH), which is a semi-permanent anticyclonic circulation at the upper troposphere covering the entire South Asian continent in boreal summer (Mason and Anderson 1963; Tao and Zhu 1964; Krishnamurti et al. 1973). SAH is maintained by sensible heating over the Tibetan Plateau and the surrounding monsoonal heating (Flohn 1957; Hoskins and Rodwell 1995; Duan and Wu 2005; Boos and Kuang 2010). Its variations were closely related to climate variabilities across the Indo-Pacific Ocean. Particularly, SAH tends to intensify following El Niño events (Zhao et al. 2009). During the El Niño decaying summer, positive sea surface temperature (SST) anomalies in the tropical Indian Ocean increase condensation heating, warm troposphere temperature and thus intensify the SAH (Huang et al. 2011; Qu and Huang 2012). Previous studies found that movements of the SAH and the subtropical high are closely tied to each other (Mason and Anderson 1963; Tao and Zhu 1964; Krishnamurti et al. 1973). This coupling of the subtropical high and the SAH further modulates the corresponding circulation patterns and thus the Asian climate and extreme events (Tao and Zhu 1964; Zhang et al. 2002, 2005; Wu et al. 2007; Wang et al. 2008; Jiang et al. 2011; Liu et al. 2013; Wei et al. 2015; Ning et al. 2017). Meanwhile, notable tropical and subtropical surface temperature contrast usually occurs in the western Pacific during different SAH phases (Zhang et al. 2005; Xue et al. 2018), indicating a possible linkage between variations in the SAH and the Pacific meridional temperature gradient. Wang et al. (2019) found the SAH is closely linked to TCG frequency in the SCS, but the related mechanism has not been revealed. Up to now, it is still unknown how the SAH modulates the underlying TCG in the SCS. It motivates us to investigate their possible relationship and to explore the related mechanism, which would enrich the understanding of variability in the SCS TCG during summer (July–September).

The remainder of this paper is organized as follows. Section 2 describes the data and methods used in this study.

Section 3 presents the leading mode of interannual variability in the SAH. Section 4 investigates impacts of the SAH on TCG frequency in the SCS and the corresponding large-scale condition anomalies. How the SAH modulates large-scale environmental parameters in the SCS is presented in Sect. 5. A summary and a discussion about possible variability source of the SAH are presented in Sect. 6.

## 2 Data and method

Best track data from the Joint Typhoon Warning Center (JTWC) were used to obtain TC information (Chu et al. 2002). TCs in this study were defined as tropical storms whose maximum wind speed reach or exceeds  $17.2 \text{ m s}^{-1}$ . The monthly and daily atmospheric data were obtained from the National Centers for Environmental Prediction (NCEP) Reanalysis (Kalnay et al. 1996). Sea surface temperature from National Oceanic and Atmospheric Administration Extended Reconstructed SST version 4 (ERSST v4) (Huang et al. 2015) was adopted to present the SST pattern linked to variations in the SAH. Monthly outgoing longwave radiation (OLR) data from NOAA (Liebmann and Smith 1996) and monthly precipitation data from the Global Precipitation Climatology Project (Adler et al. 2018) were used.

The analysis period ranges from 1979 to 2017, and we focused on the summer season (July–September, JAS) of TC activity over the SCS ( $0^{\circ}$ – $25^{\circ}$  N,  $100^{\circ}$  E– $120^{\circ}$  E). Note that the results when June–September or May–September was considered were similar to those for July–September. An 8-year high-pass Fourier filter was first applied to all observational data to isolate interannual variability. Because the conventional definition of SAH using geopotential height cannot eliminate the effect of the global warming-induced pressure level rising (Wu and Wang 2015; Wu et al. 2017), here we used 200 hPa wind field to perform multivariate Empirical Orthogonal Function (EOF) analysis (Wang 1992) to obtain the leading mode of SAH. Composite, regression, and correlation analyses were employed to present the results and statistical significance was assessed using the two-tailed Student's *t* test (Wilks 2006).

The vorticity tendency equation was adopted using daily data to diagnose the main contributor to low-level vorticity anomalies associated with variation in the SAH (Holton 1973). The vorticity tendency is balanced by four terms: the horizontal advection of the absolute vorticity (HADV), the vertical advection of the relative vorticity (VADV), the divergence (DIV) term and the tilting term (TILT):

$$\frac{\partial \xi}{\partial t} = - \left( u \frac{\partial \xi}{\partial x} + v \frac{\partial \xi}{\partial y} + w \frac{\partial \xi}{\partial z} \right) - \omega \frac{\partial \xi}{\partial p} - (f + \xi) \left( \frac{\partial u}{\partial x} + \frac{\partial v}{\partial y} \right) + \left( \frac{\partial \omega}{\partial y} \frac{\partial u}{\partial p} - \frac{\partial \omega}{\partial x} \frac{\partial v}{\partial p} \right)$$

where  $\xi$  and  $f$  represent the relative vorticity and the Coriolis parameter,  $u, v$  and  $\omega$  represent the zonal wind, meridional wind and vertical p-velocity, respectively.

### 3 The dominant mode of interannual variability in the eastern-central SAH

Figure 1a shows the leading multivariate EOF mode of 200 hPa winds over the region ( $10^{\circ}\text{N}$ – $40^{\circ}\text{N}$ ,  $90^{\circ}\text{E}$ – $120^{\circ}\text{E}$ ), which features an anomalous anti-cyclonic circulation over the south Asian continent and explained 33.7% of the total variance. We also examined the leading mode of 200 hPa wind covering the region of climatological SAH ( $10^{\circ}\text{N}$ – $40^{\circ}\text{N}$ ,  $60^{\circ}\text{E}$ – $120^{\circ}\text{E}$ ). It was found that the leading modes and the corresponding principal components (PCs) were generally similar. Here we focused on the variability of

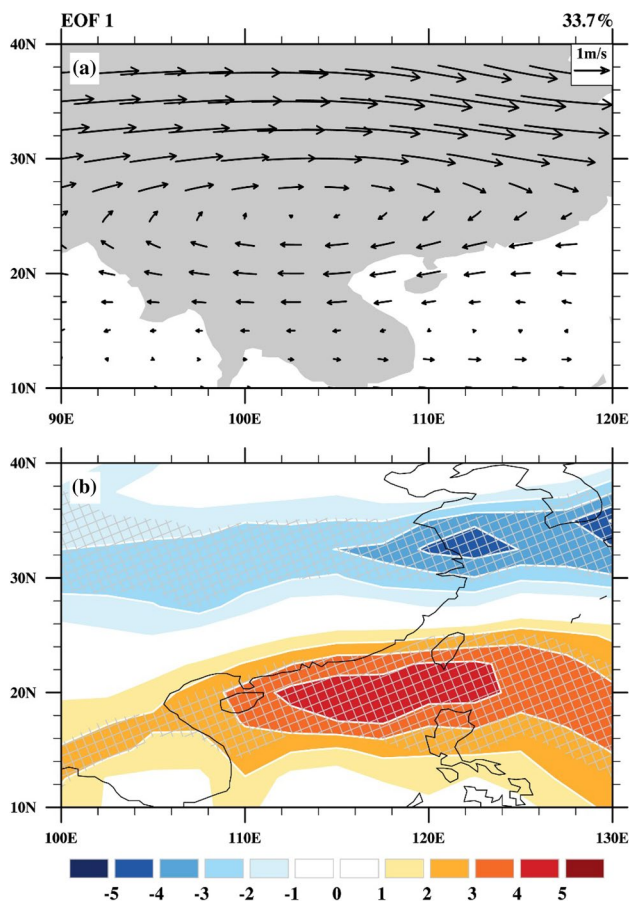


**Fig. 1** **a** The leading mode obtained by multivariate EOF analysis on the July–September mean 200 hPa wind (vectors,  $\text{m s}^{-1}$ ) over  $10^{\circ}\text{N}$ – $40^{\circ}\text{N}$ ,  $90^{\circ}\text{E}$ – $140^{\circ}\text{E}$  during 1979–2017, **b** the regressed OLR anomalies (shadings,  $\text{W m}^{-2}$ ) against the PC1 of the central eastern SAH during 1979–2017. The percentage of variance explained by the leading mode is shown on the top-right of **a**, hatched regions in **b** denote area that OLR anomalies are significant at the 90% confidence level

SAH in the vicinity of SCS to explore its influence on TCG in the SCS. In its positive phases, the leading mode serves to intensify SAH to its eastern part (Fig. 1a). Previous studies found that zonal locations of SAH experience distinct bimodality (i.e., the Tibetan mode and the Iranian mode) (Zhang et al. 2002; Wei et al. 2014; Wu et al. 2017). The leading mode actually reflects the intensity variation in the SAH Tibetan mode. Rainfall pattern over China is closely related to the zonal position of SAH (Zhang et al. 2002; Wei et al. 2014). Particularly, a strong SAH Tibetan mode is usually concurrent with enhanced rainfall in the Yangtze-Huai River valley but suppressed precipitation in South China (Zhang et al. 2002; Wei et al. 2014) due to the westward extension of subtropical high (Tao and Zhu 1964; Yang and Sun 2003; Wei et al. 2019; Krishnamurti et al. 1973). Figure 1b further shows the regressed OLR anomalies against the first PC of the eastern-central SAH (PC1) during 1979–2017. The OLR anomalies feature two zonally elongated band with negative anomalies to the north  $25^{\circ}\text{N}$  and positive anomalies to the south  $25^{\circ}\text{N}$ , which indicate enhanced rainfall in the Yangtze-Huai River valley but suppressed precipitation in South China. The suppressed precipitation in the south China hints the possible linkage between the SAH and TCG in the SCS due to the geographic proximity between the SCS and South China.

### 4 Impacts on tropical cyclogenesis and the corresponding large-scale conditions

Interannual variability in the SCS TCG frequency is tightly related to that in the leading mode of SAH variability. Particularly, the time series of PC1 and the SCS TCG frequency are significantly anti-correlated with a correlation coefficient of  $-0.71$  ( $p < 0.01$ ) during 1979–2017 (Fig. 2), suggesting about half of the interannual variance in the SCS TCG

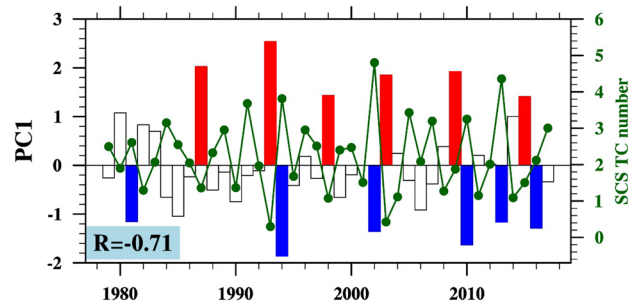


**Fig. 2** Time series of PC1 of the eastern-central SAH (bars) and TCG frequency (green line) in the SCS in July–September over 1979–2017. The correlation coefficient ( $R$ ) is shown in the down left of panel. Red (blue) bars highlight six extreme positive (negative) values of PC1

frequency can be explained by the variabilities in the leading mode. In other words, TCG in the SCS is generally enhanced (suppressed) during negative (positive) phases of the SAH leading mode.

To understand this out-phase relationship, six strong (weak) years with maximum (minimum) PC1 anomalies were picked to composite the corresponding large-scale circulation and environmental parameters. The six strong years are 1987, 1993, 1998, 2003, 2009 and 2015, and the six weak years are 1981, 1994, 2002, 2010, 2013 and 2016 (Fig. 2). The SAH experiences a significant eastward extension in strong years (Fig. 3a). The most eastward point of the 12,500-gpm contour in the strong years can extend to  $140^\circ$  E, which is  $10^\circ$  longitude more eastward than that in the weak years (Fig. 3b). As a result, their difference shows a zonally elongated anti-cyclonic circulation over the Asian continent and the western North Pacific (WNP, Fig. 3c). At the lower troposphere, the cyclonic curve associated with

monsoon trough in the SCS is much weaker in the strong years than that in the weak years (Fig. 4a, b). Meanwhile, the subtropical high ridge in the strong SAH years is more southward than that in the weak SAH years (Fig. 4a, b). The southward displacement in the subtropical high ridge indicates the westward extension and intensification of the subtropical high in the strong SAH years (Fig. 4c), which is consistent with previous studies (Tao and Zhu 1964; Yang and Sun 2003; Krishnamurti et al. 1973; Wei et al. 2019). Accompanied by these changes in large-scale circulations, TCG frequency in the SCS experiences distinctive features. In the SCS, on average, only 1.3 TCs form in the strong SAH years; while, the number is 3.7 in the weak years, about 3 times of those in strong years (Figs. 3, 4). The difference in TCG frequency is statistically significant at the 95% confidence level, probably indicating the important role of SAH

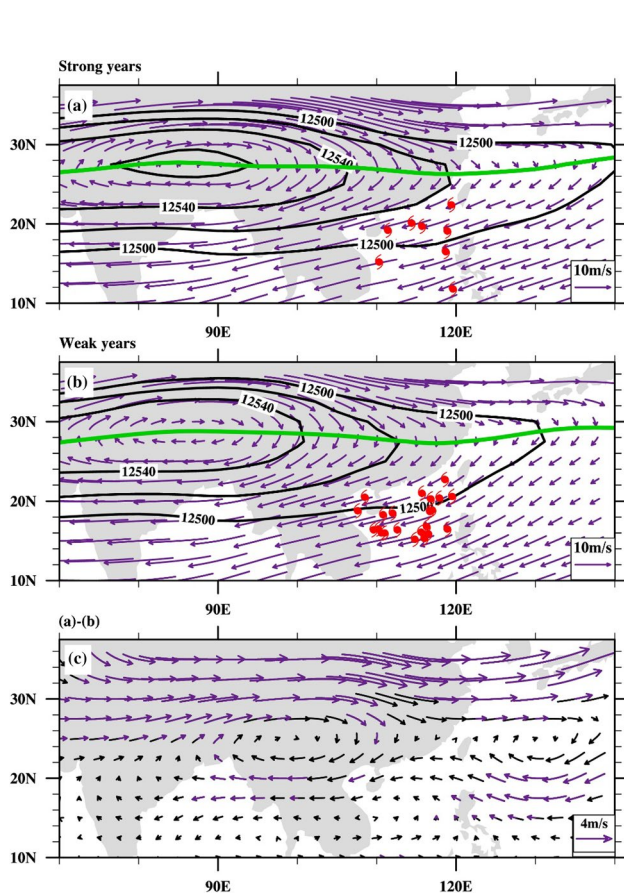


**Fig. 3** Composite mean 200 hPa winds (vectors,  $\text{m s}^{-1}$ ), geopotential height (contours, m) and the corresponding TCG locations (red symbols) in **a** the strong SAH years and **b** the weak SAH years. **c** Composite difference in 200 hPa wind (vectors,  $\text{m s}^{-1}$ ) between the strong SAH years and the weak SAH years. The thick green lines in **a** and **b** show the corresponding zero contours of 200 hPa zonal wind speed, while the purple vectors in **c** denote the wind differences that are significant at the 90% confidence level

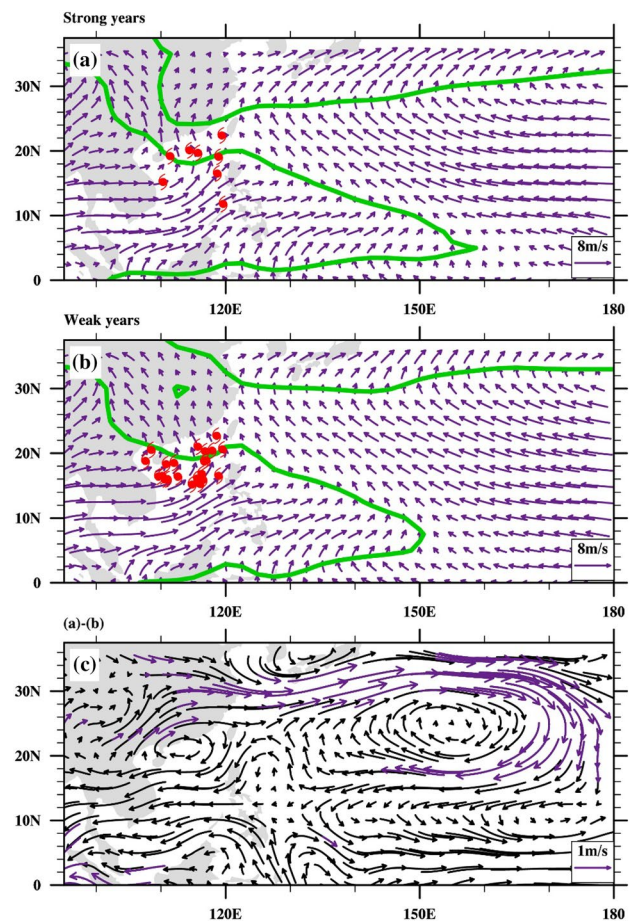


**Fig. 4** Composite 850 hPa winds (vectors,  $\text{m s}^{-1}$ ) and the corresponding TCG locations (red symbols) during **a** the strong SAH years and **b** the weak SAH years. **c** Composite difference in 850 hPa wind (vectors,  $\text{m s}^{-1}$ ) between the strong and the weak SAH years. The thick green lines in **a** and **b** show the corresponding zero contours of 850 hPa zonal wind speed, while the purple vectors in **c** denote the wind differences that are significant at the 90% confidence level

in affecting the interannual variability in TCG frequency in the SCS.

Large-scale environmental parameters play a crucial role in the processes of TCG (Gray 1968, 1979). Here we compared the differences in vertical shear of zonal wind (defined as the difference in zonal wind between 200 and 850 hPa), 850 hPa vorticity, 500 hPa vertical velocity and 600 hPa relative humidity between the strong and weak SAH years (Fig. 5). During the strong SAH years, anomalous anti-cyclonic circulation at the upper level is consistent with the enhanced subtropical westerly wind shear and tropical easterly wind shear (Fig. 5a). However, no significant difference in vertical wind shear can be identified in the SCS, which indicates the indistinctive role of vertical wind shear in the SCS TCG during different phases of SAH. At 850 hPa, an anomalous anti-cyclonic circulation and the associated negative vorticity anomalies occur in the SCS (Fig. 5b), which are unfavorable to TCG in the SCS. Moreover, vertical motion in the SCS is greatly suppressed, which can inhibit moisture transportation from low-level to the middle troposphere in strong SAH years (Fig. 5c, d). The anti-cyclonic vorticity, suppressed vertical motion, and dry middle troposphere are consistent with the suppressed TCG in the SCS during the strong SAH years. This consistency indicates changes in large-scale environments (relative vorticity, vertical motion, and mid-level humidity) are responsible for the

distinct TCG in the SCS during the two phases of the SAH leading mode.

## 5 Mechanism by which the SAH affects TC genesis in the SCS

How can the upper-level SAH modulate the low-level large-scale conditions in the SCS? Upper-level convergence/divergence associated with the SAH usually plays a vital role in modulating low-level circulation (Zhang et al. 2002; Wei et al. 2014, 2019; Ning et al. 2017). Figure 6a shows the composite 200 hPa geopotential height, wind and divergence anomalies between the strong and weak SAH years. Elongated positive geopotential height anomalies occur in the 20° N–30° N and thus anomalous convergence is found in the 20° N–30° N zonal band. The anomalous convergence zone further extends southward to the northern SCS, which is found to be linked to the two maximum geopotential height centers in 100° E–110° E and 125° E–140° E. Due to the relatively high geopotential height (i.e., great pressure gradient) over 125° E–140° E, easterlies to the south of the high geopotential center are generally greater than those over 110° E–125° E. As a result, air masses converge at the upper-level to the west of 125° E, which is favorable for anomalous descending motion due to the continuity of

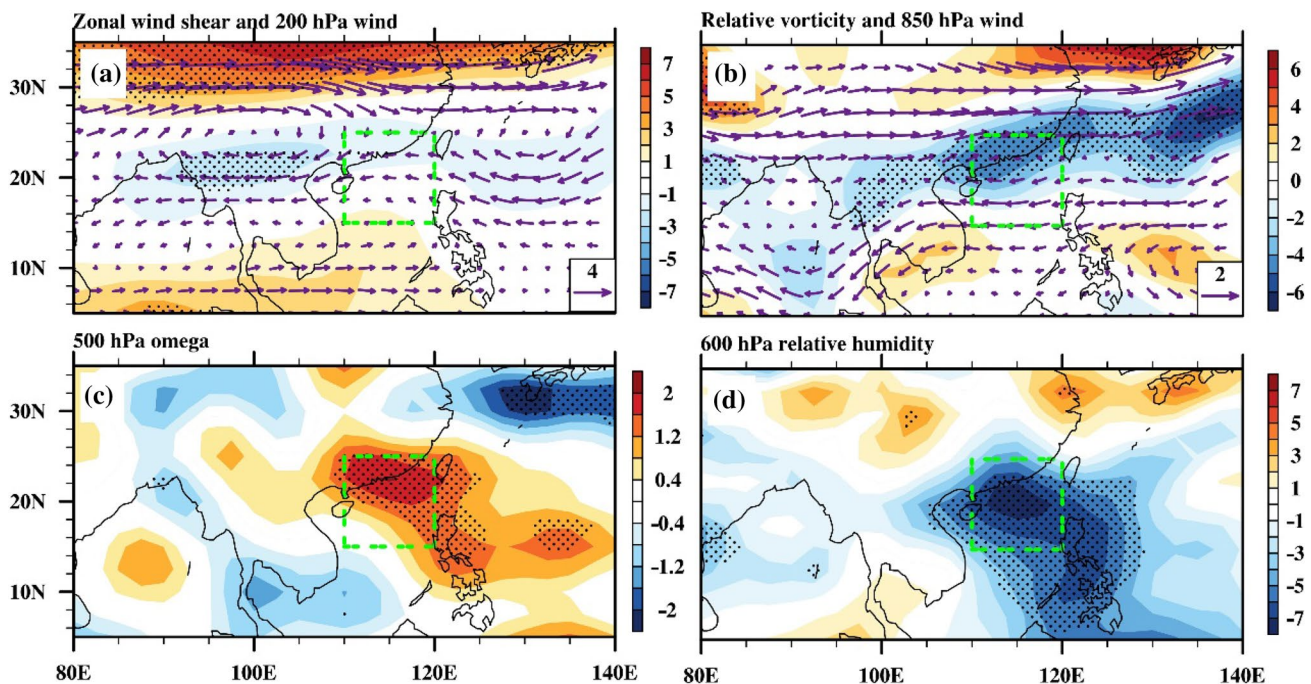


**Fig. 5** Composite differences in **a** U200–U850 (shadings,  $\text{m s}^{-1}$ ) and 200 hPa wind (vectors,  $\text{m s}^{-1}$ ), **b** 850 hPa relative vorticity (shading,  $10^{-6} \text{ s}^{-1}$ ) and 850 hPa wind (vectors,  $\text{m s}^{-1}$ ), **c** 500 hPa vertical velocity (shadings,  $10^{-2} \text{ Pa s}^{-1}$ ), and **d** 600 hPa relative humidity (shad-

ings, %) between the strong and the weak SAH years. Stippling marks the region where the differences are statistically significant at the 90% confidence level. The green boxes denote the northern SCS

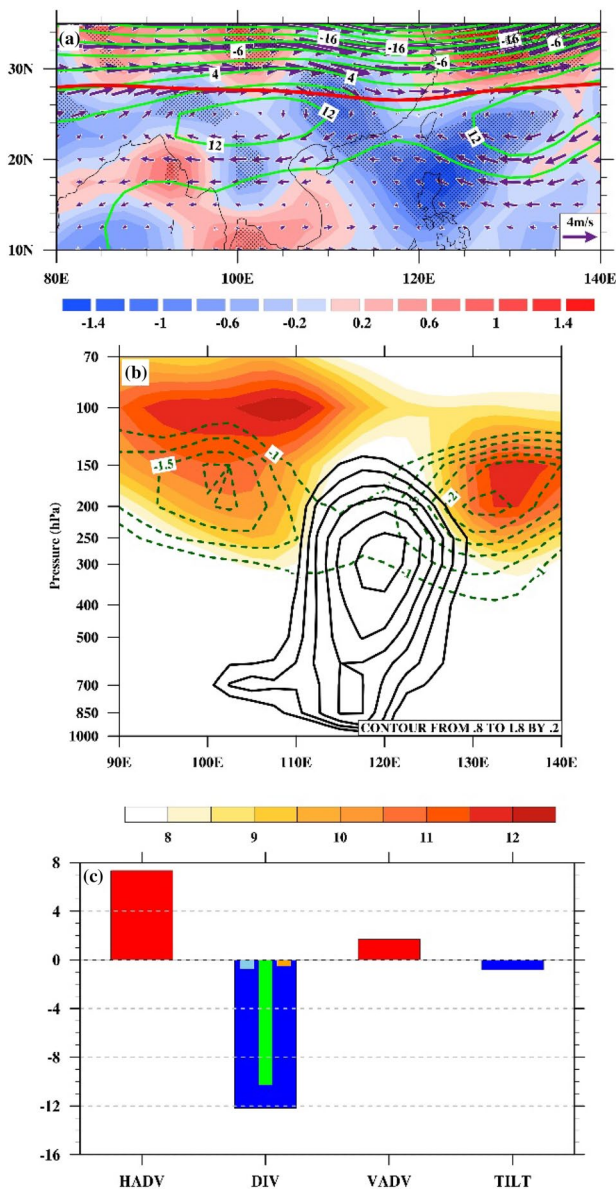


**Fig. 6** **a** Composite differences in 200 hPa geopotential height (green contours, m), wind (vectors,  $\text{m s}^{-1}$ ) and divergence (shadings,  $10^{-6} \text{ s}^{-1}$ ) between the strong SAH years and the weak SAH years. **b** Longitude-height cross section of composite  $20^{\circ} \text{ N}$ – $30^{\circ} \text{ N}$  mean geopotential height anomalies between the strong SAH years and the weak SAH years in geopotential height (color shadings, gpm),  $17.5^{\circ} \text{ N}$ – $22.5^{\circ} \text{ N}$  mean zonal wind (green contours,  $\text{m s}^{-1}$ ) and vertical velocity (black contours,  $10^{-2} \text{ Pa s}^{-1}$ ). **c** Composite differences in the horizontal advection term (HADV,  $10^{-12} \text{ s}^{-2}$ ), divergence term (DIV,  $10^{-12} \text{ s}^{-2}$ ), vertical advection term (VADV,  $10^{-12} \text{ s}^{-2}$ ), and tilting term (TILT,  $10^{-12} \text{ s}^{-2}$ ) in the vorticity equation averaged over  $15^{\circ} \text{ N}$ – $25^{\circ} \text{ N}$ ,  $110^{\circ} \text{ E}$ – $120^{\circ} \text{ E}$  at 850 hPa between the strong SAH years and the weak SAH years. Contributions of three sub-terms of the divergence term (anomalous absolute vorticity multiplied by climatological convergence, climatological absolute vorticity multiplied by anomalous convergence and anomalous absolute vorticity multiplied by anomalous convergence) are shown by light blue bar, green bar and orange bar, respectively

atmosphere. Such a linkage can be also found in the longitude-height cross-section of geopotential height and vertical motion anomalies (Fig. 6b). In the strong SAH years, two maximums in geopotential height are found in the upper troposphere and two maximum centers of upper-level easterly occur to its south. Accordingly, zonal winds converge between the two maximum centers, leading to the anomalous descending motion in the SCS. The descending motion and the related weakened moisture transportation from low-level to middle troposphere serve to suppress TCG in the SCS during strong SAH years. Meanwhile, the westerly trough in the East Asia (north of the SAH) favors the anomalous convergence to its east and thus may contribute to the anomalous vertical motion in the SCS. However, the base of the anomalous westerly trough can only extend to about  $25^{\circ} \text{ N}$ , thus its related upper-level convergence is generally confined to north to  $20^{\circ} \text{ N}$ , which may play a secondary role in variation in vertical motion in the SCS. The results suggest that the spatial structure of the SAH-related geopotential height or the wind anomalies is the key factor modulating the vertical motion in the SCS. It means that the unique spatial structure of the SAH leading mode plays a crucial role in large-scale environmental parameters in the SCS and thus the corresponding TCG. One may query about the relative importance of two anti-cyclonic centers to the anomalous large-scale environment and TCG in the SCS. We further examined the leading mode of 200 hPa wind over  $10^{\circ} \text{ N}$ – $40^{\circ} \text{ N}$ ,  $120^{\circ} \text{ E}$ – $140^{\circ} \text{ E}$  (western Pacific (WP) leading mode), which shows an anti-cyclonic circulation (figure not shown) and is consistent with the composite results based on the SAH leading mode (Figs. 5a, 6a). The corresponding PC is significantly correlated with the PC1 of the SAH leading mode ( $r=0.78$ ), indicating an in-phase variation in the two modes. However, correlation coefficient between the PC1 of the WP leading mode and the SCS TCG frequency ( $r=-0.47$ ) is much lower than that of PC1 of the SAH leading mode ( $r=-0.71$ ). The weaker correlation is consistent with the weaker composite large-scale environment anomalies between the strong and the weak WP years in the SCS. Thus, the WP anti-cyclone and its related large-scale condition anomalies are less influential than the SAH in affecting the SCS TCG.

A remaining issue is how the upper-level SAH induces changes in the low-level vorticity (Fig. 5b). Figure 6c shows the composite differences in the four terms that contribute to the negative 850 hPa vorticity anomalies in the northern SCS ( $15^{\circ} \text{ N}$ – $25^{\circ} \text{ N}$ ,  $110^{\circ} \text{ E}$ – $120^{\circ} \text{ E}$ ) between the strong SAH years and the weak SAH years. It can be seen that the divergence term is the major contributor to the negative vorticity anomalies in the northern SCS (Fig. 6c). We further decomposed the anomalous divergence term

into (1) anomalous absolute vorticity multiplied by climatological convergence; (2) climatological absolute vorticity multiplied by anomalous convergence, and (3) anomalous absolute vorticity multiplied by anomalous convergence. It can be seen that the climatological absolute vorticity multiplied by anomalous low-level convergence is the main driver of the low-level negative vorticity anomalies (Fig. 6c). During the strong SAH years, prominent convergence that occurs in the upper-level is concurrent with low-level divergence in the SCS. Because cyclonic vorticity prevails in the SCS in summer, the anomalous low-level divergence acts to increase the anti-cyclonic vorticity. In summary, during the strong (weak) SAH years, the SAH-related upper-level convergence (divergence) is conducive to anomalous descending (ascending) motion and low-level divergence (convergence) in the SCS, decreasing (increasing) the mid-level humidity and low-level vorticity and thus suppressing (enhancing) TCG in the SCS. How can the central-eastern SAH anomaly maintain itself through the entire summer? An anomalous signal in atmospheric circulation, by itself, cannot persist for months, while anomalous signals in lower boundary (e.g., land and ocean) can induce atmospheric deviations persisting for months to years (Shukla 1998; Wang et al. 2005). Here we found that variations in the leading mode of SAH are closely linked to the meridional surface temperature gradient across the WNP (Fig. 7a). The surface warming in the tropical WNP tends to warm the tropical tropospheric temperature and increase the tropospheric thickness between 200 and 850 hPa, while the surface cooling in the subtropical WNP cools the subtropical troposphere and decreases the tropospheric thickness (Fig. 7b). As a result, positive geopotential height anomalies occur to the south of 35° N and negative geopotential height anomalies occur to the north of 35° N at 200 hPa (Fig. 7c), enhancing the anti-cyclonic circulation to the south of 35° N at upper-level and thus intensify the SAH. The enhanced SAH is conducive to anomalous descending motion, which is favorable for the low-level anti-cyclonic circulation and thus decrease TCG in the SCS (Fig. 7a). On the other hand, the suppressed convection in the SCS can reduce cloudiness and increase the downward solar radiation at the surface (Fig. 8a), re-enforcing the surface warming through a positive SST-cloud-shortwave radiation feedback (Philander et al. 1996). Hence the meridional temperature gradient over the WNP is enhanced. The positive feedback between the SAH and the WNP meridional temperature gradients can maintain both the enhanced meridional temperature gradients and SAH through summer. In summary, the increased meridional surface temperature gradient, the intensified upper-level SAH and the low-level anticyclonic circulation act as an interactive system, collectively suppressing TCG in the SCS during

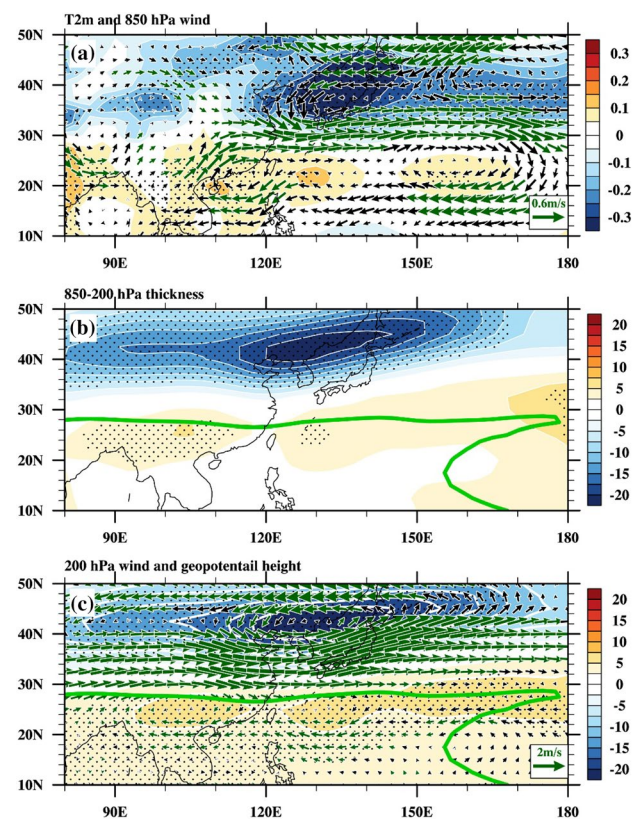


**Fig. 7** Regressed **a** surface temperature (shadings, °C) and 850 hPa wind (vectors,  $\text{m s}^{-1}$ ), **b** 850–200 hPa tropospheric geopotential thickness (shadings, m), **c** 200 hPa geopotential height (shadings, gpm) and wind (vectors,  $\text{m s}^{-1}$ ) anomalies with respect to the PC1 of the eastern-central SAH during 1979–2017. The green lines in **b** and **c** denotes the zero contour of climatological mean zonal wind. Stippling marks the region where the differences are statistically significant at the 90% confidence level

the strong SAH years. Opposite processes are in function during the weak SAH years.

## 6 Summary and discussion

While the linkages between the SAH and Asian climate are extensively studied, impacts of the SAH on the underlying TCG in the SCS remain unexplored. Here we found that the leading mode of eastern-central SAH and TCG number in the SCS during July–September are significantly correlated with a correlation coefficient of  $-0.71$  during 1979–2017. Six strong and six weak SAH years were contrasted. In the SCS, on average, only 1.3 TCs form in the strong SAH years; while, the number is 3.7 in the weak years, about 3 times of those in strong years. The suppressed TCG in the SCS during strong SAH years is in accordance with the unfavorable large-scale conditions, including reduced vertical motion, mid-level humidity, and low-level vorticity. During the

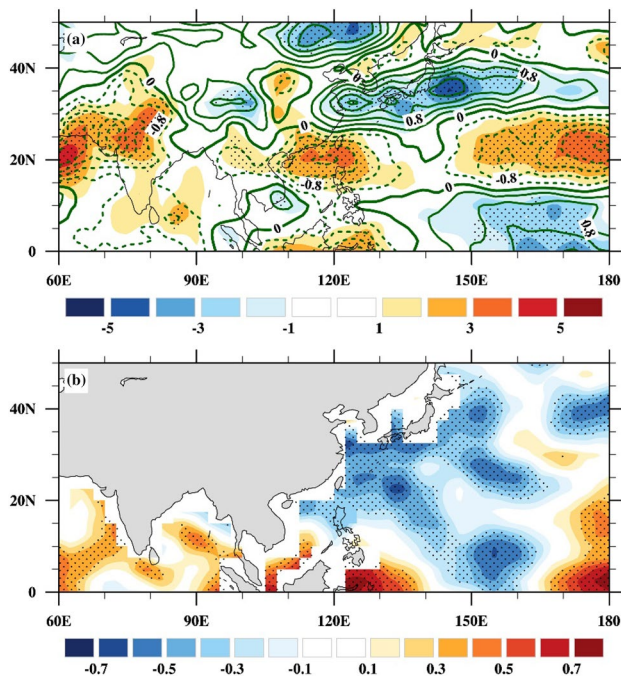


**Fig. 8** **a** Regressed downward solar radiation flux at surface anomalies (shadings,  $\text{W m}^{-2}$ ) and total cloud cover (green contours, %) against the PC1 of the eastern-central SAH during 1979–2017. **b** Correlation map between the JAS mean SST and precipitation. Stippling marks the region where the regressed anomalies (**a**) or the correlation coefficients (**b**) are statistically significant at the 90% confidence level

strong SAH years, the upper-level convergence, the related descending motion and low-level divergence occur in the SCS, decreasing mid-level humidity and low-level vorticity and thus suppressing TCG in the SCS. During the opposite phase of SAH, the processes that enhance SCS TCG are just opposite. We find that the variations in the leading mode of eastern-central SAH are coupled to the meridional gradient in surface temperature over the western North Pacific. An enhanced meridional surface temperature gradient can increase the meridional gradient in 200 hPa geopotential height and thus intensify the SAH. Meanwhile, the intensified SAH and the related descending motion, in turn, reinforce the meridional surface temperature gradient through positive SST-cloud-shortwave radiation feedback. The positive feedback between the SAH and the WNP meridional temperature gradients provides persisting large-scale circulation anomalies that influence the TCG in the SCS from July through September. The present results suggest that the precursors that are known to be linked to the SAH intensity variation can be used for the seasonal prediction of TCG in the SCS.

One may concern the role of the pre-winter ENSO condition in variations of the SAH leading mode due to the similar low-level circulation anomalies (Wang et al. 2000; Xie et al. 2009; Huang et al. 2011). It indicates

a possibility that El Niño leads to changes in the SAH, WNP SST gradient and SCS TCG together, which results in good relationship among the three. Here we found that time series of the December–February Niño index is insignificantly correlated with the SAH leading mode ( $r = 0.16$ ) and the July–September TC genesis frequency in the SCS ( $r = -0.13$ ). It is suggested that variations in the leading SAH mode and the July–September TC genesis frequency in the SCS are statistically independent of the pre-winter ENSO condition. Another possible concern is why the surface temperature anomalies cannot directly modulate TCG in the SCS via changing the lower-level circulation as the surface temperature anomalies may stimulate significant change in large-scale circulation via changing convective heating (Gill 1980). However, the surface temperature anomalies in the WNP cannot be simply treated as a forcing due to the notable air-sea interaction in this region (Wang et al. 2005). Figure 8b further shows the correlation map between the JAS mean SST and precipitation over the WNP. Consistently negative correlation can be found across the WNP, which indicates that it is the atmosphere (reduced cloudiness) affects SST through increasing the downward solar radiation, rather than the SST affects the atmosphere in this region (Wang et al. 2005). The passive role of SST in this region cannot be considered as forcing to the atmospheric large-scale circulation and thus to the variations of the TCG in the SCS. It should be noted that the passive role of ocean temperature mainly refers to the negative relationship between SST and the local precipitation (Fig. 8b). However, in term of tropospheric temperature, ocean warming can increase the equivalent potential temperature in the atmospheric boundary layer (Emanuel et al. 1994), which can further heat the atmospheric column, elevate the pressure level and ultimately strengthen the upper-level SAH. The results show that upper-tropospheric circulation associated with SAH variability plays an important role in low-level circulation over the SCS by modulating vertical motions. On the other hand, the anomalous low-level circulation and the related convective heating anomalies can also modulate vertical motions over the SCS and thus the SCS TCG. Both the aforementioned upper-level and low-level processes can contribute to the anomalous large-scale conditions that are important for TCG in the SCS. The relative importance of the upper-level and low-level processes needs further examination.

**Acknowledgements** This study was jointly supported by the National Key R&D Program of China (2019YFC1510201), the National Natural Science Foundation of China (Grant Nos. 42075031, 41730961 and 41922033) and the National Key R&D Program of China (Grant No. 2016YFA0600401).

## References

- Adler RF et al. (2018) The Global Precipitation Climatology Project (GPCP) monthly analysis (New Version 2.3) and a review of 2017 global precipitation. *Atmosphere* (Basel) 9:138. <https://doi.org/10.3390/atmos9040138>
- Boos WR, Kuang Z (2010) Dominant control of the South Asian monsoon by orographic insulation versus plateau heating. *Nature* 463:218–222. <https://doi.org/10.1038/nature08707>
- Briegleb LM, Frank WM (1997) Large-scale influences on tropical cyclogenesis in the Western North Pacific. *Mon Weather Rev* 125:1397–1413. [https://doi.org/10.1175/1520-0493\(1997\)125%3c1397:LSIOTC%3e2.0.CO;2](https://doi.org/10.1175/1520-0493(1997)125%3c1397:LSIOTC%3e2.0.CO;2)
- Chen G (2011) How does shifting Pacific ocean warming modulate on tropical cyclone frequency over the South China Sea? *J Clim* 24:4695–4700. <https://doi.org/10.1175/2011JCLI4140.1>
- Chu J-H, Sampson CR, Levine AS, Fukada E (2002) The joint typhoon warning center tropical cyclone best-tracks, 1945–2000. Naval Research Lab, Monterey
- Du Y, Yang L, Xie S-P (2011) Tropical Indian Ocean influence on Northwest Pacific tropical cyclones in summer following strong El Niño\*. *J Clim* 24:315–322. <https://doi.org/10.1175/2010JCLI3890.1>
- Duan AM, Wu GX (2005) Role of the Tibetan Plateau thermal forcing in the summer climate patterns over subtropical Asia. *Clim Dyn* 24:793–807. <https://doi.org/10.1007/s00382-004-0488-8>
- Emanuel KA, David Neelin J, Bretherton CS (1994) On large-scale circulations in convecting atmospheres. *Q J R Meteorol Soc* 120:1111–1143. <https://doi.org/10.1002/qj.49712051902>
- Flohn H (1957) Large-scale aspects of the “Summer Monsoon” in South and East Asia. *J Meteorol Soc Jpn Ser II* 35A:180–186. [https://doi.org/10.2151/jmsj1923.35a.0\\_180](https://doi.org/10.2151/jmsj1923.35a.0_180)
- Gill A (1980) Some simple solutions for heat-induced tropical circulation. *Q J R Meteorol Soc* 106:447–462
- Goh AZC, Chan JCL (2010) Interannual and interdecadal variations of tropical cyclone activity in the South China Sea. *Int J Climatol* 30:827–843. <https://doi.org/10.1002/joc.1943>
- Gray WM (1968) Global view of the origin of tropical disturbances and storms. *Mon Weather Rev* 96:669–700
- Gray WM (1979) Hurricanes: their formation, structure and likely role in the tropical circulation. In: Shaw DB (ed) *Meteorology over tropical oceans*. Royal Meteorological Society, Bracknell, pp 155–218
- Holton JR (1973) An introduction to dynamic meteorology. *Am J Phys* 41:752–754
- Hoskins BJ, Rodwell MJ (1995) A model of the Asian summer monsoon. Part I: the global scale. *J Atmos Sci* 52:1329–1340
- Huang G, Qu X, Hu K (2011) The impact of the tropical Indian Ocean on South Asian High in boreal summer. *Adv Atmos Sci* 28:421–432. <https://doi.org/10.1007/s00376-010-9224-y>
- Huang B et al. (2015) Extended reconstructed sea surface temperature version 4 (ERSST.v4). Part I: upgrades and intercomparisons. *J Clim* 28:911–930. <https://doi.org/10.1175/JCLI-D-14-00006.1>
- Jiang X, Li Y, Yang S, Wu R (2011) Interannual and interdecadal variations of the South Asian and western Pacific subtropical highs and their relationships with Asian-Pacific summer climate. *Meteorol Atmos Phys* 113:171–180. <https://doi.org/10.1007/s00703-011-0146-8>
- Kalnay E et al. (1996) The NCEP/NCAR 40-year reanalysis project. *Bull Am Meteorol Soc* 77:437–471
- Kossin JP, Emanuel KA, Camargo SJ (2016) Past and projected changes in western north Pacific tropical cyclone exposure. *J Clim* 29:5725–5739. <https://doi.org/10.1175/JCLI-D-16-0076.1>
- Krishnamurti TN et al. (1973) Tibetan high and upper tropospheric tropical circulations during northern summer. *Bull Am Meteorol Soc* 54:1234–1250. <https://doi.org/10.1175/1520-0477-54.12.1234>
- Li RCY, Zhou W (2014) Interdecadal change in South China Sea tropical cyclone frequency in association with zonal sea surface temperature gradient. *J Clim* 27:5468–5480. <https://doi.org/10.1175/JCLI-D-13-00744.1>
- Liebmann B, Smith AC (1996) Description of a complete (interpolated) outgoing longwave radiation dataset. *Bull Am Meteorol Soc*, 1275–1277. <https://www.jstor.org/stable/26233278?seq=1> (Accessed 30 Sept 2020).
- Liu B, Wu G, Mao J, He J (2013) Genesis of the south Asian high and its impact on the Asian summer monsoon onset. *J Clim* 26:2976–2991. <https://doi.org/10.1175/jcli-d-12-00286.1>
- Mason RB, Anderson CE (1963) The development and decay of the 100-MB. Summertime anticyclone over Southern Asia. *Mon Weather Rev* 91:3–12. [https://doi.org/10.1175/1520-0493\(1963\)091%3c0003:TDADOT%3e2.3.CO;2](https://doi.org/10.1175/1520-0493(1963)091%3c0003:TDADOT%3e2.3.CO;2)
- Ning L, Liu J, Wang B (2017) How does the South Asian high influence extreme precipitation over eastern China? *J Geophys Res Atmos* 122:4281–4298. <https://doi.org/10.1002/2016JD026075>
- Peduzzi P, Chatenoux B, Dao H, De Bono A, Herold C, Kossin J, Mouton F, Nordbeck O (2012) Global trends in tropical cyclone risk. *Nat Clim Change* 2:289–294. <https://doi.org/10.1038/nclimate1410>
- Philander SGH, Gu D, Halpern D, Lambert G, Lau NC, Li T, Pacanowski RC (1996) Why the ITCZ is mostly north of the equator. *J Clim* 9:2958–2972. [https://doi.org/10.1175/1520-0442\(1996\)009%3c2958:WTIIMN%3e2.0.CO;2](https://doi.org/10.1175/1520-0442(1996)009%3c2958:WTIIMN%3e2.0.CO;2)
- Qu X, Huang G (2012) An Enhanced influence of tropical Indian Ocean on the South Asia high after the late 1970s. *J Clim* 25:6930–6941. <https://doi.org/10.1175/jcli-d-11-00696.1>
- Shukla J (1998) Predictability in the midst of chaos: a scientific basis for climate forecasting. *Science* 282:728–731. <https://doi.org/10.1126/science.282.5389.728>
- Tao S, Zhu F (1964) The 100 mb flow patterns in southern Asia in summer and its relation to the advance and retreat of the west2 Pacific subtropical anticyclone over the far east. *Acta Meteorol Sin* 34:385–396
- Wang B (1992) The vertical structure and development of the ENSO anomaly mode during 1979–1989. *J Atmos Sci* 49:698–712. [https://doi.org/10.1175/1520-0469\(1992\)049%3c0698:TVSADO%3e2.0.CO;2](https://doi.org/10.1175/1520-0469(1992)049%3c0698:TVSADO%3e2.0.CO;2)
- Wang B, Chan JCL (2002) How strong ENSO events affect tropical storm activity over the western North Pacific. *J Clim* 15:1643–1658. [https://doi.org/10.1175/1520-0442\(2002\)015%3c1643:HSEEAT%3e2.0.CO;2](https://doi.org/10.1175/1520-0442(2002)015%3c1643:HSEEAT%3e2.0.CO;2)
- Wang C, Wang B (2019) Tropical cyclone predictability shaped by western Pacific subtropical high: integration of trans-basin sea surface temperature effects. *Clim Dyn* 53:2697–2714. <https://doi.org/10.1007/s00382-019-04651-1>
- Wang C, Wu L (2016) Interannual shift of the tropical upper-tropospheric trough and its influence on tropical cyclone formation over the western North Pacific. *J Clim* 29:4203–4211. <https://doi.org/10.1175/JCLI-D-15-0653.1>
- Wang C, Wu L (2018a) Future changes of the monsoon trough: sensitivity to sea surface temperature gradient and implications for tropical cyclone activity. *Earth's Future* 6:919–936. <https://doi.org/10.1029/2018EF000858>
- Wang C, Wu L (2018b) Projection of North Pacific tropical upper-tropospheric trough in CMIP5 models: implications for changes in tropical cyclone formation locations. *J Clim* 31:761–774. <https://doi.org/10.1175/JCLI-D-17-0292.1>

- Wang B, Wu R, Fu X (2000) Pacific-East Asian teleconnection: how does ENSO affect East Asian climate? *J Clim* 13:1517–1536. [https://doi.org/10.1175/1520-0442\(2000\)013%3c1517:PEATHD%3e2.0.CO;2](https://doi.org/10.1175/1520-0442(2000)013%3c1517:PEATHD%3e2.0.CO;2)
- Wang B, Ding Q, Fu X, Kang I-S, Jin K, Shukla J, Doblas-Reyes F (2005) Fundamental challenge in simulation and prediction of summer monsoon rainfall. *Geophys Res Lett* 32:15711. <https://doi.org/10.1029/2005GL022734>
- Wang G, Su J, Ding Y, Chen D (2007) Tropical cyclone genesis over the south China sea. *J Mar Syst* 68:318–326. <https://doi.org/10.1016/J.JMARSYS.2006.12.002>
- Wang B, Bao Q, Hoskins B, Wu G, Liu Y (2008) Tibetan Plateau warming and precipitation changes in East Asia. *Geophys Res Lett*. <https://doi.org/10.1029/2008gl034330>
- Wang L, Huang R, Wu R (2013) Interdecadal variability in tropical cyclone frequency over the South China Sea and its association with the Indian Ocean sea surface temperature. *Geophys Res Lett* 40:768–771
- Wang X, Zhou W, Li C, Wang D (2014) Comparison of the impact of two types of El Niño on tropical cyclone genesis over the South China Sea. *Int J Climatol* 34:2651–2660. <https://doi.org/10.1002/joc.3865>
- Wang C, Wang B, Wu L (2019) A region-dependent seasonal forecasting framework for tropical cyclone genesis frequency in the Western North Pacific. *J Clim* 32:8415–8435. <https://doi.org/10.1175/JCLI-D-19-0006.1>
- Wei W, Zhang R, Wen M, Rong X, Li T (2014) Impact of Indian summer monsoon on the South Asian High and its influence on summer rainfall over China. *Clim Dyn* 43:1257–1269. <https://doi.org/10.1007/s00382-013-1938-y>
- Wei W, Zhang R, Wen M, Kim B-JJ, Nam J-CC (2015) Interannual variation of the South Asian high and its relation with Indian and east asian summer monsoon rainfall. *J Clim* 28:2623–2634. <https://doi.org/10.1175/JCLI-D-14-00454.1>
- Wei W, Zhang R, Wen M, Yang S, Li W (2019) Dynamic effect of the South Asian high on the interannual zonal extension of the western North Pacific subtropical high. *Int J Climatol*. <https://doi.org/10.1002/joc.6160>
- Wilks DS (2006) Statistical methods in the atmospheric sciences. Academic Press, London
- Wu L, Wang C (2015) Has the western Pacific subtropical high extended westward since the late 1970s? *J Clim* 28:5406–5413. <https://doi.org/10.1175/JCLI-D-14-00618.1>
- Wu G et al. (2007) The influence of mechanical and thermal forcing by the Tibetan Plateau on Asian climate. *J Hydrometeorol* 8:770–789
- Wu L, Wang C, Wang B (2015) Westward shift of western North Pacific tropical cyclogenesis. *Geophys Res Lett* 42:1537–1542. <https://doi.org/10.1002/2015GL063450>
- Wu L, Feng X, Liang M (2017) Insensitivity of the summer South Asian high intensity to a warming Tibetan Plateau in modern reanalysis datasets. *J Clim* 30:3009–3024. <https://doi.org/10.1175/JCLI-D-16-0359.1>
- Xie S-P, Hu K, Hafner J, Tokinaga H, Du Y, Huang G, Sampe T (2009) Indian Ocean capacitor effect on Indo-Western Pacific climate during the summer following El Niño. *J Clim* 22:730–747. <https://doi.org/10.1175/2008JCLI2544.1>
- Xue X, Chen W, Chen S, Feng J (2018) PDO modulation of the ENSO impact on the summer South Asian high. *Clim Dyn* 50:1393–1411. <https://doi.org/10.1007/s00382-017-3692-z>
- Yang H, Sun S (2003) Longitudinal displacement of the subtropical high in the western Pacific in summer and its influence. *Adv Atmos Sci* 20:921–933. <https://doi.org/10.1007/BF02915515>
- Zhang Q, Wu G, Qian Y (2002) The bimodality of the 100 hPa South Asia high and its relationship to the climate anomaly over East Asia in summer. *J Meteorol Soc Jpn Ser II* 80:733–744. <https://doi.org/10.2151/jmsj.80.733>
- Zhang P, Yang S, Kousky VE (2005) South Asian high and Asian-Pacific-American climate teleconnection. *Adv Atmos Sci* 22:915–923
- Zhang Q, Wu L, Liu Q (2009) Tropical cyclone damages in China 1983–2006. *Bull Am Meteorol Soc* 90:489–496. <https://doi.org/10.1175/2008BAMS2631.1>
- Zhao P, Zhang X, Li Y, Chen J (2009) Remotely modulated tropical-North Pacific ocean-atmosphere interactions by the South Asian high. *Atmos Res* 94:45–60. <https://doi.org/10.1016/J.ATMOSRES.2009.01.018>
- Zuki ZM, Lupo AR (2008) Interannual variability of tropical cyclone activity in the southern South China Sea. *J Geophys Res* 113:D06106. <https://doi.org/10.1029/2007JD009218>

**Publisher's Note** Springer Nature remains neutral with regard to jurisdictional claims in published maps and institutional affiliations.